Intrinsic electronic properties of high-quality wurtzite InN

H. Eisele,[1,*] J. Schuppang,[1] M. Schnedler,[2] M. Duchamp,[2,3] C. Nenstiel,[1] V. Portz,[2] T. Kure,[1] M. Bügler,[1] A. Lenz,[1] M. Dähne,[1] A. Hoffmann,[1] S. Gwo,[4] S. Choi,[5] J. S. Speck,[5] R. E. Dunin-Borkowski,[2,3] and Ph. Ebert[2]

[1]*Technische Universität Berlin, Institut für Festkörperphysik, Hardenbergstraße 36, 10623 Berlin, Germany*

[2]*Peter Grünberg Institut, Forschungszentrum Jülich Gmb H, 52428 Jülich, Germany*

[3]*Ernst-Ruska-Centre, Forschungszentrum Jülich Gmb H, 52428 Jülich, Germany*

[4]*Department of Physics, National Tsing-Hua University, Hsinchu 30013, Taiwan*

[5]*Materials Department, University of California, Santa Barbara, California 93106, USA*

(Received 30 June 2016; revised manuscript received 21 September 2016; published 16 December 2016)

Recent reports suggested that InN is a highly unusual III-V semiconductor, whose behavior fundamentally differs from that of others. We therefore analyzed its intrinsic electronic properties on the highest available quality InN layers, demonstrating the absence of electron accumulation at the $(10\bar{1}0)$ cleavage surface and in the bulk. The bulk electron density is governed solely by dopants. Hence, we conclude that InN acts similarly to the other III-V semiconductors and previously reported intriguing effects are related to low crystallinity, surface decomposition, nonstoichiometry, and/or In adlayers.

DOI: 10.1103/PhysRevB.94.245201

I. INTRODUCTION

In recent years, high interest has developed around indium nitride (InN) due to measurements and calculations suggesting highly intriguing electronic properties, such as the existence of an electron accumulation in the bulk conduction band [1–6], an extremely large electron affinity [7,8], or the supposed impossibility of obtaining effectively *p*-doped surfaces [9]. Even superconductivity was reported [10–12]. According to these reports, InN appears to be a highly unusual semiconductor, differing fundamentally from all other binary compound semiconductors.

Unfortunately, until now macroscopic InN single crystal bulk material has not been available. Hence, experiments need to be performed either at heteroepitaxially grown layers [2,7,10,13–18] or at nanostructures [4,8,19]. However, heteroepitaxially grown layers typically contain a high density of defects, while nanostructures show interface and/or surface effects, both leading to a rather complex data interpretation. Regrettably, until now, all experimental measurements were performed on such samples. In order to review the *intrinsic* electronic properties of InN, experiments need to be performed on high-quality single crystal material with low defect density and low strain, offering access to actual intrinsic electronic properties.

In this contribution, we probe the electronic properties of high-quality thick heteroepitaxial wurtzite InN layers grown on GaN(0001). The high material quality is proven by Raman spectroscopy (RS), photoluminescence (PL), and high-resolution transmission electron microscopy (HR-TEM). The electronic properties are determined using cross-sectional scanning tunneling microscopy (XSTM) and spectroscopy (XSTS). We demonstrate that no intrinsic electron accumulation is present either at the surface or in the bulk. The bulk free electron density is solely governed by dopants and defects but not by an intrinsic material property. High-quality InN appears to be as conventional as all the other binary III-V semiconductors. All other reported effects, including superconductivity, are related to low crystallinity, surface decomposition, nonstoichiometry, and/or In adlayers.

II. EXPERIMENTAL RESULTS AND DISCUSSION

We investigated 1 μm thick InN layers grown along the *c* direction on free-standing *n*-type GaN pseudosubstrates using plasma-assisted molecular beam epitaxy. The *n*-type InN layers exhibited a Si doping concentration of a few 10^{18} cm^{-3}. For further details see Ref. [20].

A. Structural quality

First, we assess the crystalline quality of the InN layers. Figures 1(a) and 1(b) illustrate the XSTM results. The GaN pseudosubstrate exhibits perfect cleavage without (or with only a few) steps. In contrast, at the InN/GaN interface suddenly a high density of surface steps form and propagate along the *c* direction into the InN layer. The line profile in Fig. 1(b) (left frame) demonstrates that these steps have a height of 1 ML (monolayer). The width of the elongated terraces is typically 2–5 nm directly at the interface. Overview XSTM images show that with increasing distance from the interface some of the steps annihilate, leading to 40 to 50 nm wide terraces.

The appearance of steps at the interface indicates the presence of interface dislocations intersecting the *m*-plane cleavage surface [21]. The step height shows that the Burgers vectors of the interface dislocations have a component of 1 ML along the *m* direction, i.e., $\pm a/2[10\bar{1}0]$. The annihilation of such steps demonstrates that dislocations with oppositely oriented Burgers vectors are present.

In order to determine the in-plane component of the Burgers vector, we prepared cross-sectional HR-TEM specimens by ion beam milling. A final cleaning was performed with low-energy Ar^+-ion bombardment (0.5 eV) at liquid

*holger.eisele@physik.tu-berlin.de

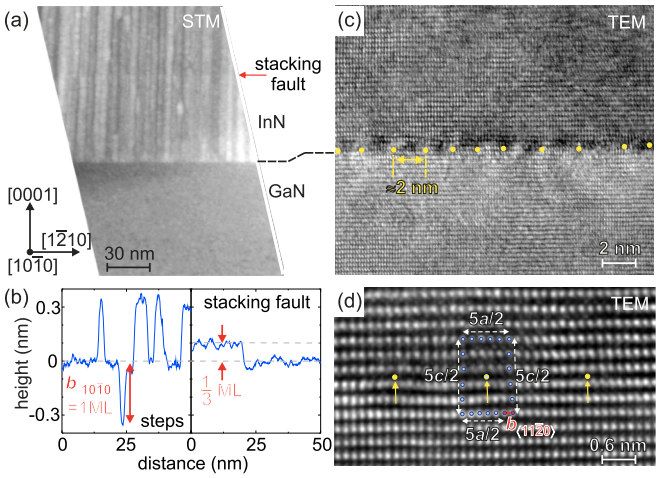

FIG. 1. Cross-sectional scanning tunneling and transmission electron microscopy of the InN layer on GaN. (a) Constant-current XSTM image of the InN/GaN interface region measured at +4.5 V sample voltage and 40 pA tunnel current. A high density of steps oriented along the [0001] direction is present at the InN(10$\bar{1}$0) cleavage surface. Each step starts at the interface, demonstrating the presence of interface dislocations with out-of-plane burgers vector components $\underline{b}_{\perp} = \pm a/2[10\bar{1}0]$, as illustrated in the left part of frame (b). (c) HR-TEM image along the [10$\bar{1}$0] direction providing an overview over the InN/GaN interface. At the interface a dislocation network (cores marked by yellow points) is present. (d) Atomic resolution aberration corrected HR-TEM image showing the interface dislocations at higher magnification. The Burgers circuit yields the in-plane component of the Burgers vector to be $\underline{b}_{\parallel} = a/6[1\bar{2}10]$. The interface dislocations are hence edge dislocations with a Burgers vector of the type $\underline{b} = a/3\langle 11\bar{2}0\rangle$. In the InN layer, in few cases stacking faults were observed, as indicated by the (red) arrow in (a). The stacking faults induce a height shift of 1/3 ML, as illustrated in the right part of frame (b).

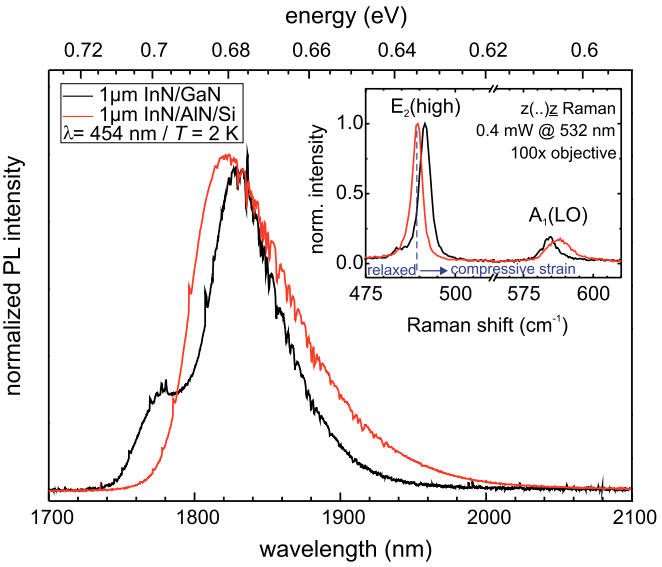

FIG. 2. Photoluminescence spectra of the InN/GaN(0001) sample (black) as well as of a comparable InN/AlN/Si(111) sample (red). Inset: Corresponding Raman spectra.

N_2 temperature using a Fischione Nanomill system. Structural investigations were performed using a FEI Titan TEM equipped with a spherical aberration corrector at the image plane. In the overview TEM image of the interface region [Fig. 1(c)], a more or less regular pattern of dislocations is detected at the InN/GaN interface. In the imaged area, the individual dislocations have a separation of about 2 nm. The interface dislocations are shown at higher magnification in the atomic resolution aberration corrected HR-TEM image in Fig. 1(d). Each atomic contrast arises from one Ga/In column along the [10$\bar{1}$0] direction. Hence, the separation between neighboring contrast maxima corresponds to $a/2$ and $c/2$, with a and c being the lattice constants along the [1$\bar{2}$10] and [0001] directions, respectively. The in-plane component of the Burgers vector, illustrated using the Burgers circuit in Fig. 1(d), is found to be $a/6[1\bar{2}10]$. Hence, the dislocation network at the interface is composed of pure edge dislocations with Burgers vectors of the type $a/3\langle 11\bar{2}0\rangle$. The average dislocation separation observed in HR-TEM images matches well the average step separation in XSTM images of 2–5 nm directly at the interface. These values are consistent with an interface dislocation network for the ~11.2% lattice mismatch of InN/GaN(0001). Note that, due to symmetry reasons, one should expect each equivalent Burgers vector orientation to occur on average with equal frequency. In the nonatomically resolved XSTM image, however, only such dislocations were detected, whose Burgers vectors have an out-of-plane component (four of the six possible a-type Burgers vectors).

Besides the interface dislocation network, we detected only very few dislocations within the InN layer: We found sometimes stacking faults on the c-plane giving rise to a step on the cleavage plane of 1/3 ML oriented along the a direction. The arrow in Fig. 1(a) marks such a stacking fault and the height profile in Fig. 1(b) (right) illustrates the height offset of 1/3 ML. This suggests that most of the strain is relaxed directly at the interface. Hence, one can expect that the InN layer further away from the interface is essentially strain free and of high quality.

In order to corroborate this local information we investigated the samples by RS and PL, averaging the information on a large area. Figure 2 displays PL spectra of the InN/GaN(0001) sample and, for comparison, of an InN/AlN/Si(111) sample. The spectra exhibit pronounced differences: While the PL spectrum of the InN/AlN/Si(111) shows a single peak at 0.68 eV with a line shape typical for degenerated semiconductors, the one of the InN/GaN(0001) sample exhibits a double peak structure (peaks at 0.677 and 0.695 eV). The high energy peak at 0.695 eV originates from band-to-band transitions (Mahan excitons) caused by the Burstein-Moss shift [22–24], which are only visible in high-quality layers [25]. The lower energy peaks of both samples (0.68 and 0.677 eV) can be assigned to point defect bands near the conduction band. The luminescence of both samples originate, however, from different defects/impurities, since their energy and full width half maximum (FWHM) differ. Note that if the luminescence peaks would have identical energies but different blue shifts due to different compressive strain, then a reversal of the peak positions occurs, in contradiction to the observation. For the InN/GaN(0001)

sample, the PL intensity drops from low-temperature to room-temperature to about 1/8.

The RS of InN/GaN(0001) (black curve in the inset of Fig. 2) shows a narrow E_2(high)-mode at 491.51 cm^{-1} with a FWHM of 3.34 cm^{-1}. For comparison, the RS of the InN/AlN/Si(111) sample (red curve) [14] has the E_2(high)-mode at 489.36 cm^{-1} with a FWHM of 3.02 cm^{-1}. The position of the E_2(high)-mode is slightly shifted between both samples, with that of the InN/AlN/Si(111) sample being closer to the relaxed value (dashed vertical line). Hence, the InN/GaN(0001) sample is slightly compressively strained.

The A_1(LO)-mode of InN/AlN/Si(111) is broadened and shifted to higher wave numbers in comparison to that of InN/GaN(0001). This effect, arising from longitudinal phonon plasmon coupling, indicates a higher free carrier concentration (CC) for the InN/AlN/Si(111) sample. A calculation of the shift between the A_1(LO)-modes of both samples suggests a 3 to 4 times lower CC in the Si-doped InN/GaN(0001) layer as compared to unintentionally doped InN/AlN/Si(111), where a CC of 2×10^{18} cm^{-3} was measured [14]. Thus, the CC of the InN/GaN(0001) layer is $\sim(5-8)\times10^{17}$ cm^{-3}, in good agreement with the Si doping of a few 10^{18} cm^{-3}, considering that only a fraction of the Si dopants are actually thermally ionized. This suggests that the luminescence peak at 0.677 eV is primarily originating from Si doping. Hence, the InN/GaN(0001) layer has a high crystalline quality (narrow E_2-mode) and a free CC determined by the Si doping but not by unintentional defects.

B. Electronic properties

Now we turn to the electronic properties of the InN layers. Figure 3(a) shows XSTS spectra measured at the *m*-plane cleavage surface of the GaN substrate (red) and the InN layer (blue). The XSTS spectra were acquired with a PtIr tip at constant tip-sample separation, which was fixed by a set current of 35 pA and set voltages of +2.5 V and +1.0 V for GaN and InN, respectively [14,27]. Taking into account the different band gaps, these set voltages lead to roughly equal tip-sample separations on both materials. Both spectra exhibit clear semiconducting properties: The voltage range, in which the tunnel current is below the detection limit of ∼1 pA, can be seen best with a logarithmic current scale in Fig. 3(b). It is about 0.7 V (2.0 V) wide for InN(GaN). These voltage ranges without tunnel current (called here apparent band gap) arise from the presence of a band gap. Obviously, the values require a detailed explanation, which is related to the presence or absence of *extrinsic* surface states.

First, we recall the discussion of the tunneling spectra measured at GaN($10\bar{1}0$) surfaces [26,28]. GaN($10\bar{1}0$) surfaces exhibit a polarity-dependent Fermi-level pinning [28]. The cleaved GaN surface is free of surface steps [Fig. 1(a)] and hence free of *extrinsic* states. Therefore, the electric field applied between the tip and the negatively biased sample penetrates partially into the semiconductor and induces a so-called tip-induced band bending [29–31]. This leads to a downward band bending at negative voltages resulting in a *tip-induced* electron accumulation in the conduction band. The tunnel current at negative voltages is then dominated by

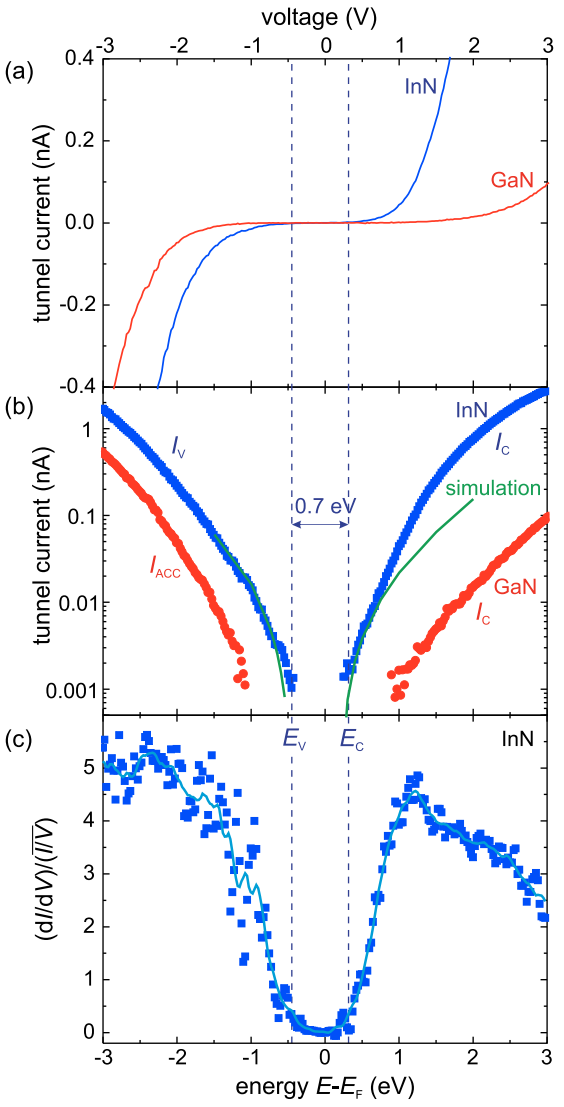

FIG. 3. Scanning tunneling spectroscopy of InN (blue) and GaN (red) ($10\bar{1}0$) surfaces. Panels (a) and (b) illustrate the tunnel current versus voltage using a linear and a logarithmic scale, respectively. The (green) solid line in (b) shows the simulated tunnel current for InN, assuming a pinning by step states in the band gap. The positive and negative branches of the tunnel current correspond to the tunneling of electrons into the conduction band (I_C) and out of the valence band (I_V), respectively, separated by the band gap of ∼0.7 eV. The Fermi energy is 0.27 eV below the conduction band edge, i.e., within the fundamental band gap. In contrast, the GaN surface is free of steps and hence the tunneling spectrum is affected by the tip-induced band bending. The band bending induces a tunnel current from the tip-induced accumulation zone in the conduction band at negative voltages (I_{ACC}), reducing the apparent band gap [26]. (c) Normalized differential conductivity $(dI/dV)/(\overline{I/V})$ derived from the tunnel spectrum in (a).

electrons tunneling out of the tip-induced electron accumulation zone. This accumulation current I_{ACC} starts already at negative voltages corresponding to energies within the band gap of GaN. Tunneling out of valence band states occurs only at larger magnitudes of negative voltages and is negligible as compared to I_{ACC} [26]. At positive voltages, the tunnel current

arises from electrons tunneling into empty conduction band states I_C. Hence, the apparent band gap of ∼2.0 eV for GaN is smaller than the fundamental bulk band gap of 3.4 eV due to the tip-induced band bending at negative sample voltages.

In contrast, the InN(10$\bar{1}$0) cleavage surface has a large density of steps starting at the misfit dislocation network at the GaN/InN interface. These steps have electronic states in the band gap and act as *extrinsic* pinning centers [32–34]. Therefore, the Fermi energy is pinned at the InN surface and no tip-induced band bending occurs. Hence, the voltage scale corresponds directly to the energy scale and the tunnel currents at positive and negative voltages arise from tunneling into the empty conduction (I_C) and filled valence band states (I_V), respectively. Thus, the band gap equals the measured voltage range without tunnel current times the electron charge, i.e., ∼0.7 eV. This agrees well with the bulk band gap of InN [35,36] and is further confirmed by our PL results.

In order to corroborate the interpretation above, the tunnel current is calculated following Ref. [37], using a band gap of 0.67 eV [35,36] as well as effective hole and electron masses of 0.5 and 0.11 m_e, respectively [38]. The extrinsic pinning centers at the InN surface due to steps are modeled as a half-filled Gaussian distribution, being energetically located 0.27 eV below the conduction band edge (FWHM = 0.1 eV). Assuming an average step separation of ∼3 nm [arising from the misfit dislocations at the InN/GaN(0001) interface] and one defect state per lattice constant along the step edge, an extrinsic defect state density of $\sim 5\times10^{13}$ cm^{-2} is obtained and used for the calculation.

The calculated tunnel current is shown in Fig. 3(b) as a solid (green) line. From fitting the absolute amount of the tunnel current, a tip-sample separation of 0.79 nm is obtained. The resulting valence and conduction band edge positions of $E_V = -0.40$ eV and $E_C = +0.27$ eV are indicated by the (blue) vertical dashed lines. The calculated tunnel current agrees well with the initial slopes and onset voltages of the measured data. The calculation corroborates that at negative voltages the current arises from electrons tunneling from the filled valence band states. At positive voltages, electrons tunnel into the empty conduction band states.

The experimentally measured and the simulated XSTS spectra at the InN(10$\bar{1}$0) cleavage surface demonstrate that the Fermi energy is about 0.27 eV below conduction band edge *within* the fundamental band gap. If an electron accumulation would exist at the surface, then the Fermi energy would have to be energetically located above the conduction band edge. Thus, there is no electron accumulation at the stoichiometric *m*-plane cleavage surface. There exists even no (tip-induced) electron accumulation with a positively biased tip in close proximity to the negatively biased InN(10$\bar{1}$0) sample surface.

On the basis of these observations we discuss the absence of an intrinsic electron accumulation zone in InN and the concept of a charge neutrality level. For this, we have to distinguish between the bulk Fermi level position and the surface band bending. First, we address the surface band bending: The thus-far-reported electron accumulation zones are due to a downward surface band bending of ∼0.7−1.5 eV [2,13]. This magnitude of band bending requires a pinning level deep in the conduction band at the surface. If this pinning is caused by an intrinsic surface state or adlayers, its density of states is typically given by one state per unit cell, i.e., $\sim 5\times10^{14}$ cm^{-2}. Our density of defect states at step edges is ten times lower and hence cannot compensate a pinning by intrinsic surface states or adlayers. Thus, our midgap pinning by step states excludes any presence of pinning by intrinsic surface states or adlayers and therefore indicates that no intrinsic electron accumulation layer can exist.

Second, the *bulk* carrier concentration (and thus Fermi level) can be extracted from RS (and PL) in Fig. 2, since both probe in the ∼100 nm depth range. Due to the Si doping of the InN layer, the surface band bending is screened within ∼10 nm below the surface. Hence, the majority of the PL and Raman signals originate from bulklike regions. The RS and PL shown in Fig. 2 and discussed above yielded a carrier concentration of the InN/GaN(0001) sample that is governed solely by the Si doping but not by unintentional defects. Hence, it is not of intrinsic origin. Therewith, a charge neutrality level deep in the conduction band is not appropriate for describing the properties of our high-quality InN sample. Furthermore, the compensation of the *n*-type doping by rather small surface defect concentrations demonstrates the fundamental possibility of *p*-type doping in InN.

In addition, the differential conductivity in Fig. 3(c) shows no indications of *intrinsic* surface states within the fundamental band gap. Thus, one is faced with the classical situation of a non-polar III-V semiconductor surface, where the bulk band gap is free of intrinsic surface states. This agrees well with theoretical calculations of the band structure of the InN(10$\bar{1}$0) surface [39], where the filled and empty surface states are located energetically within the valence and conduction band, respectively.

Our results raise the question regarding why an electron accumulation is detected frequently at InN surfaces and said to be a universal *intrinsic* effect. The surface-sensitive measurement techniques depend directly on the surface quality. Here we cleaved the samples *in situ* in ultra-high vacuum, leading to clean and stoichiometric surfaces. There is also one report about InN nanowire as-grown side wall facets without surface electron accumulation [19]. But all other previously used preparation techniques, requiring thermal treatments (or/and ion bombardment) rather lead to non-stoichiometric surfaces covered by In adlayers [13], also predicted theoretically to be the stable surface configuration [40]. Such metallic 1 to 2 ML thick In adlayers pin the surface (resulting in an electron accumulation). On polar surfaces the electron accumulation is related to In adlayers, too, and can be reduced to almost zero/flat band conditions [16] when In is removed from the InN(000$\bar{1}$) surface. Thus, In adlayers lead indeed to the frequently detected electron accumulation. The In adlayers may also be the origin of the detected superconductivity, since its reported Curie temperature between 2.3 and 3.97 K [10,12] fits well to that of bulk indium of 3.4 K [41].

III. CONCLUSION

In conclusion, clean, high-quality, stoichiometric, and bulklike InN(10$\bar{1}$0) exhibits no *intrinsic* surface states within the band gap, no intrinsic electron accumulation at the surface, and

a bulk free electron concentration governed solely by dopants and defects. Electron accumulation needs to be assigned to *extrinsic* effects, as, e.g., the decomposition of the surface and/or the formation of In adatom layers. From this point of view, InN appears to be as conventional as all other binary III-V semiconductors.

ACKNOWLEDGMENTS

The authors thank the Deutsche Forschungsgemeinschaft for support under the Projects Eb197/5 and Ei788/2 as well as by the Collaborative Reserach Center Sfb 787, Project TP A4.

[1] S. X. Li, K. M. Yu, J. Wu, R. E. Jones, W. Walukiewicz, J. W. Ager, W. Shan, E. E. Haller, H. Lu, and W. J. Schaff, Phys. Rev. B **71**, 161201 (2005).
[2] P. D. C. King, T. D. Veal, C. F. McConville, F. Fuchs, J. Furthmüller, F. Bechstedt, P. Schley, R. Goldhahn, J. Schörmann, D. J. As, K. Lischka, D. Muto, H. Naoi, Y. Nanishi, H. Lu, and W. J. Schaff, Appl. Phys. Lett. **91**, 092101 (2007).
[3] W. M. Linhart, T. D. Veal, P. D. C. King, G. Koblmüller, C. S. Gallinat, J. S. Speck, and C. F. McConville, Appl. Phys. Lett. **97**, 112103 (2010).
[4] E. Calleja, J. Grandal, M. A. Sánchez-García, M. Niebelschütz, V. Cimalla, and O. Ambacher, Appl. Phys. Lett. **90**, 262110 (2007).
[5] I. Mahboob, T. D. Veal, C. F. McConville, H. Lu, and W. J. Schaff, Phys. Rev. Lett. **92**, 036804 (2004).
[6] T. Nagata, G. Koblmüller, O. Bierwagen, C. S. Gallinat, and J. S. Speck, Appl. Phys. Lett. **95**, 132104 (2009).
[7] J. W. Ager, N. Miller, R. E. Jones, K. M. Yu, J. Wu, W. J. Schaff, and W. Walukiewicz, Phys. Status Solidi B **245**, 873 (2008).
[8] C.-T. Kuo, K.-K. Chang, H.-W. Shiu, C.-R. Liu, L.-Y. Chang, C.-H. Chen, and S. Gwo, Appl. Phys. Lett. **99**, 122101 (2011).
[9] W. Walukiewicz, J. W. A. III, K. M. Yu, Z. Liliental-Weber, J. Wu, S. X. Li, R. E. Jones, and J. D. Denlinger, J. Phys. D **39**, R83 (2006).
[10] T. Inushima, V. Mamutin, V. Vekshin, S. Ivanov, T. Sakon, M. Motokawa, and S. Ohoya, J. Cryst. Growth **227–228**, 481 (2001).
[11] T. Inushima, D. K. Maude, N. Kato, H. Lu, W. J. Schaff, R. Tauk, Y. Meziani, S. Ruffenach, O. Briot, W. Knap, B. Gil, H. Miwa, A. Yamamoto, D. Muto, and Y. Nanishi, AIP Conf. Proc. **893**, 137 (2007).
[12] E. Tiras, M. Gunes, N. Balkan, R. Airey, and W. J. Schaff, Appl. Phys. Lett. **94**, 142108 (2009).
[13] C.-L. Wu, H.-M. Lee, C.-T. Kuo, C.-H. Chen, and S. Gwo, Phys. Rev. Lett. **101**, 106803 (2008).
[14] Ph. Ebert, S. Schaafhausen, A. Lenz, A. Sabitova, L. Ivanova., M. Dähne, Y.-L. Hong, S. Gwo., and H. Eisele, Appl. Phys. Lett. **98**, 062103 (2011).
[15] K. A. Rickert, A. B. Ellis, F. J. Himpsel, H. Lu, W. Schaff, J. M. Redwing, F. Dwikusuma, and T. F. Kuech, Appl. Phys. Lett. **82**, 3254 (2003).
[16] C.-T. Kuo, S.-C. Lin, K.-K. Chang, H.-W. Shiu, L.-Y. Chang, C.-H. Chen, S.-J. Tang, and S. Gwo, Appl. Phys. Lett. **98**, 052101 (2011).
[17] C. S. Gallinat, G. Koblmüller, J. S. Brown, and J. S. Speck, J. Appl. Phys. **102**, 064907 (2007).
[18] K. Wang, T. Yamaguchi, T. Araki, E. Yoon, and Y. Nanishi, Jpn. J. Appl. Phys. **50**, 01AE02 (2011).
[19] S. Zhao and Z. Mi, Phys. Status Solidi C **11**, 412 (2014).
[20] O. Bierwagen, S. Choi, and J. S. Speck, Phys. Rev. B **84**, 235302 (2011).
[21] Ph. Ebert, L. Ivanova, S. Borisova, H. Eisele, A. Laubsch, and M. Dähne, Appl. Phys. Lett. **94**, 062104 (2009).
[22] M. Feneberg, J. Däubler, K. Thonke, R. Sauer, P. Schley, and R. Goldhahn, Phys. Rev. B **77**, 245207 (2008).
[23] M. Feneberg, J. Däubler, K. Thonke, R. Sauer, P. Schley, and R. Goldhahn, Phys. Status Solidi C **6**, S385 (2009).
[24] R. Kirste, M. P. Hoffmann, E. Sachet, M. Bobea, Z. Bryan, I. Bryan, C. Nenstiel, A. Hoffmann, J.-P. Maria, R. Collazo, and Z. Sitar, Appl. Phys. Lett. **103**, 242107 (2013).
[25] B. Arnaudov, T. Paskova, E. M. Goldys, S. Evtimova, and B. Monemar, Phys. Rev. B **64**, 045213 (2001).
[26] Ph. Ebert, L. Ivanova, and H. Eisele, Phys. Rev. B **80**, 085316 (2009).
[27] L. Ivanova, S. Borisova, H. Eisele, M. Dähne, A. Laubsch, and Ph. Ebert, Appl. Phys. Lett. **93**, 192110 (2008).
[28] M. Schnedler, V. Portz, H. Eisele, R. E. Dunin-Borkowski, and P. Ebert, Phys. Rev. B **91**, 205309 (2015).
[29] R. M. Feenstra and J. A. Stroscio, J. Vac. Sci. Technol. B **5**, 923 (1987).
[30] M. Wenderoth, M. A. Rosentreter, K. J. Engel, A. J. Heinrich, M. A. Schneider, and R. G. Ulbrich, Europhys. Lett. **45**, 579 (1999).
[31] R. Dombrowski, C. Steinebach, C. Wittneven, M. Morgenstern, and R. Wiesendanger, Phys. Rev. B **59**, 8043 (1999).
[32] S. Gaan, G. He, R. M. Feenstra, J. Walker, and E. Towe, J. Appl. Phys. **108**, 114315 (2010).
[33] M. Heinrich, C. Domke, Ph. Ebert, and K. Urban, Phys. Rev. B **53**, 10894 (1996).
[34] P. Capiod, T. Xu, J. P. Nys, M. Berthe, G. Patriarche, L. Lymperakis, J. Neugebauer, P. Caroff, R. E. Dunin-Borkowski, Ph. Ebert, and B. Grandidier, Appl. Phys. Lett. **103**, 122104 (2013).
[35] V. Davydov, A. Klochikhin, V. Emtsev, S. Ivanov, V. Vekshin, F. Bechstedt, J. Furthmüller, H. Harima, A. Mudryi, A. Hashimoto, A. Yamamoto, J. Aderhold, J. Graul, and E. Haller, Phys. Status Solidi B **230**, R4 (2002).
[36] J. Wu, W. Walukiewicz, K. M. Yu, J. W. Ager, E. E. Haller, H. Lu, W. J. Schaff, Y. Saito, and Y. Nanishi, Appl. Phys. Lett. **80**, 3967 (2002).
[37] M. Schnedler, V. Portz, P. H. Weidlich, R. E. Dunin-Borkowski, and Ph. Ebert, Phys. Rev. B **91**, 235305 (2015).
[38] C. P. Foley and T. L. Tansley, Phys. Rev. B **33**, 1430 (1986).
[39] C. G. Van de Walle and D. Segev, J. Appl. Phys. **101**, 081704 (2007).
[40] D. Segev and C. G. Van de Walle, Surf. Sci. Lett. **601**, L15 (2007).
[41] J. Daunt, A. Horseman, and K. Mendelssohn, Lond. Edinb. Dublin Philos. Mag. J. Sci. **27**, 754 (1939).